PCCP

PAPER

View Article Online
View Journal | View Issue

Cite this: *Phys. Chem. Chem. Phys.*, 2022, **24**, 24793

syn-Cryptophanes: macrocyclic compounds with optimized characteristics for the design of ^{129}Xe NMR-based biosensors†

Estelle Léonce,[a] Thierry Brotin[b] and Patrick Berthault *[a]

Received 12th August 2022,
Accepted 30th September 2022

DOI: 10.1039/d2cp03714a

rsc.li/pccp

A new water-soluble xenon host system with great promise for the ^{129}Xe NMR-based biosensing approach is presented: the *syn*-cryptophane-222-hexacarboxylate. It compares favorably with its already known *anti* diastereomer, on the one hand, and with cucurbit[6]uril, on the other hand, in particular in terms of xenon binding constant and xenon in–out exchange, a key parameter for the efficiency of the most sensitive HyperCEST method.

Introduction

In an approach pioneered by the group of Pines in 2001,[1] spin hyperpolarized xenon is encapsulated in molecular systems functionalized with ligands in order to target specific biological receptors. Xenon reversibly complexed in these host molecules has a specific chemical shift and an in–out exchange that gives the method a high sensitivity. All this combines to constitute a powerful NMR molecular imaging tool.[2,3]

Since the first studies in this field, cryptophanes, cage molecules consisting of two cyclotribenzylene (CTB) groups linked by three alkoxy chains, have been most often used in this purpose. A wide range of applications was covered, concerning the targeting of biological receptors[4–7] (here fluorescence detection usually accompanies ^{129}Xe NMR) or small molecules such as metal cations,[8–10] biothiols,[11] detection of temperature[12] or pH variations.[13,14] Water-soluble cryptophanes have been synthesized, based on the structure of *anti*-cryptophane-A, among which is compound **1** shown in Fig. 1.[15] But the use of cryptophane derivatives in this approach was questioned by some researchers, due to the difficulty of their synthesis, their poor solubility in aqueous media, the presence of enantiomers and also the fact that the xenon in–out exchange rate was lower than with other host systems. Indeed this dynamic parameter is key in the sensitivity of the detection method based on Chemical Exchange Saturation Transfer (Hyper-CEST).[16] For instance, cucurbit[6]uril derivatives were preferred to cryptophanes despite the difficulty of functionalizing them with biological ligands.[17–20] Native cucurbit[6]uril (compound **3** of Fig. 1) has even been chosen as a proof-of-concept for *in vivo* detection.[21,22]

However, the synthesis of *syn*-cryptophane-B (the diastereomeric molecule of cryptophane-A) has recently been achieved.[23] Interestingly, this compound opens up new possibilities for designing water-soluble molecular receptors for xenon after appropriate modification of its backbone. Thus, from the synthesis of *syn*-cryptophane-B, many different derivatives can be produced. The water-soluble compound **2**, shown in Fig. 1, is an example among others and is the diastereomer of compound **1** which has a good affinity for xenon in aqueous solution.

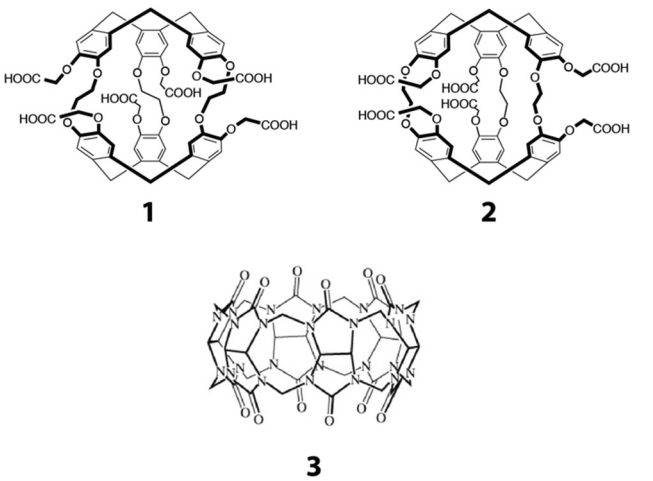

Fig. 1 Xenon hosts used in this study. **1**: *anti*-cryptophane-222 hexa carboxylate; **2**: *syn*-cryptophane-222-hexacarboxylate. **3**: cucurbit[6]uril.

[a] *NIMBE, CEA, CNRS, Université de Paris Saclay, CEA Saclay, 91191 Gif-sur-Yvette, France. E-mail: patrick.berthault@cea.fr*
[b] *ENSL, CNRS, Laboratoire de Chimie UMR 5182, 46 allée d'Italie, 69364 Lyon, France*

† Electronic supplementary information (ESI) available: Synthetical pathway to cryptophane **2**, ^{1}H and ^{13}C spectra of the intermediates, HSQC, HMBC of **2**, ^{129}Xe spectra of compounds **1** and **3**, ^{1}H spectra comparing **1** and **2**, **1** and **3** in different experimental conditions, pulse sequence to measure the depolarization rate, simulation of the effect of the rf pulse. See DOI: https://doi.org/10.1039/d2cp03714a

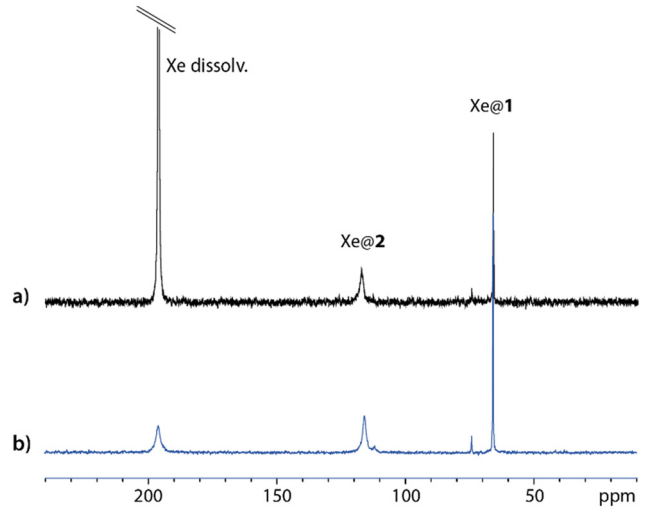

Fig. 2 One-scan ^{129}Xe NMR spectra obtained on a mixture of compounds **1** (0.51 mM) and **2** (0.49 mM) in D_2O + εNaOD, at (a) high xenon concentration, (b) low xenon concentration (sum of three experiments). B_0 = 11.7 T; T = 298 K.

The synthetic pathway for cryptophane **2** and its characterization as well as this of the intermediates is given in the ESI† (Fig. S1–S11). Unlike other *syn*-cryptophanes (except for those containing nitrogen groups on the linkers or as aromatic substituents[24,25]), xenon in the presence of compound **2** exhibits a slow exchange situation at 11.7 T and room temperature, *i.e.* the xenon exchange in and out of the cryptophane cavity is slower than the xenon resonance frequency difference between these environments.

Fig. 2 displays one-scan ^{129}Xe NMR spectra recorded with laser-polarized gas dissolved in a quasi-equimolar solution mixture of compounds **1** and **2**. After calibration of the free dissolved xenon signal at 196 ppm, while xenon caged in **1** (Xe@**1**) resonates near 65 ppm in agreement with ref. 15, a third signal at 116 ppm shows the encapsulation of xenon in **2** (Xe@**2**, as confirmed in Fig. S12, ESI†). The larger linewidth for Xe@**2** than for Xe@**1** is a first indication of a higher xenon in–out exchange rate. This prompted us to evaluate comparatively with other xenon hosts the performance of this new member of the *syn*-cryptophane family as a basis for ^{129}Xe NMR-based biosensors.

Results and discussion

Introducing low amounts of xenon inside the solution – the situation displayed in Fig. 2b – avoids saturation of the xenon cages, and thus opens the way to estimation of the affinity constant. In this purpose, comparison is made with cryptophane **1**, whose binding constant with xenon has been reported to 6800 M^{-1} at 298 K.[15] Fig. 2b displays the hyperpolarized ^{129}Xe spectrum for a mixture with equimolar concentrations of cryptophanes. The respective integrals of the caged xenon signals are very close, revealing that the affinity constants are similar. In any case they are far higher than the binding constant of cucurbit[6]uril with xenon, reported to 210 M^{-1}.[17] This parameter dictates the instantaneous occupancy rate of the host molecule in xenon, and such high values for compounds **1** and **2** ensure that there are not too many guest competitors in solution. This competition effect can be detrimental for *in vivo* experiments, as already noticed by McHugh *et al.* in the case of cucurbituril derivatives.[22]

But other factors play into the performance of a xenon host for potential ^{129}Xe NMR-based biosensors. When dissolving as is cryptophane **1** in water, the canonical crown–crown conformation is not the only form present as it coexists with crown-saddle forms (see Fig. S13b of the ESI† and ref. 15). Strong bubbling during several hours (for instance with helium) or pressurization of the NMR sample with several bars of xenon during days was shown necessary to recover the canonical form.

This shows that the non-canonical forms are not prone to encapsulate xenon when it is present in low concentration, which can be detrimental to the biosensing approach. At the contrary, cryptophane **2** dissolved in water exhibits a very simple ^{1}H spectrum (see Fig. S13a of the ESI†), expected for the canonical form of C_{3h} symmetry.

Note that non-canonical forms are also observed in the preparation of intermediates required for the synthesis of the *anti*-**1** compound. This therefore considerably complicates the synthesis and purification of derivatives of *anti* configuration and biosensors made from these compounds. Thus, the absence of non-canonical form with *syn*-**2** and its congeners seems to be an asset for the preparation of new NMR-based biosensors.

Also, from the comparison of the ^{1}H NMR spectra of an equimolar mixture of cryptophanes **1** and **2** recorded just after dissolution, after solution degassing and after introduction of xenon (Fig. 3), several conclusions can be drawn. First, the signals that are the most affected – the most sharpened – by the degassing belong to cryptophane **1**. This effect, particularly

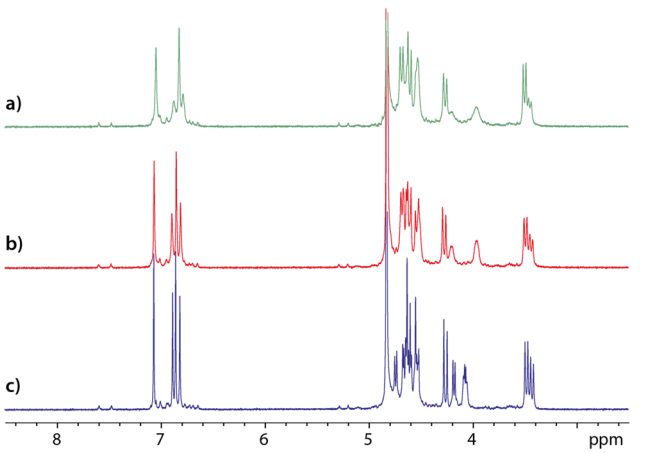

Fig. 3 ^{1}H NMR spectrum of a mixture of cryptophanes **1** and **2** in D_2O (B_0 = 11.7 T; T = 298 K). (a) as is; (b) after having degassed the solution; (c) after addition of *ca.* 5 mM of xenon. Concentration of **1** = 51 μM; concentration of **2** = 49 μM. Small signals visible on spectra (a–c) are characteristic of the 'non-canonical' forms of compound **1** (see text).

observable on the aromatic protons, indicates that cryptophane **1** must complex paramagnetic oxygen molecules dissolved in water. To check this hypothesis, in a separate experiment we have added pure oxygen gas into NMR tubes containing degassed solutions of either cryptophane **1**, cryptophane **2** or a mixture of cryptophanes **1** and **2** (Fig. S14 and S15 of the ESI†). Comparison of the ^{1}H spectra confirms the specific complexation of dissolved oxygen by cryptophane **1**. This is neither to be the case for **2**, not for cucurbit[6]uril **3**, while cucurbit[5]uril has been shown to slowly but strongly trap oxygen.[26]

The addition of xenon in solution further sharpens the ^{1}H NMR signals, but in an equivalent way for both cryptophanes. In the last spectrum displayed in Fig. 3c, thus even after solution degassing and addition of xenon, the relative integrals of the aromatic protons reveal that only *ca.* 75% of the cryptophane **1** is in the canonical crown–crown conformation. On this spectrum, notice also the narrowing of the linker proton signals (near 4 ppm) for both cryptophanes when xenon is present. This undoubtedly indicates a modification of the dynamics of these linkers and an adaptation of the host molecule structure to xenon.

Using a dedicated pulse sequence, we have assessed the detectability of each compound *via* indirect detection based on the xenon in–out exchange. In the so-called HyperCEST approach,[27] the intensity of the signal of free xenon is observed after saturation at a given frequency. If the saturation is applied near the resonance of the caged xenon frequency, the magnetization decreases quickly due to the exchange, and depletion of the main signal is observed. With a saturation of strength $\omega_1 = \gamma B_1$ applied exactly on-resonance, the depolarization rate is given by:[28,29]

$$\lambda_{on}(\omega_1) \approx f \cdot k_{out} \frac{{\omega_1}^2}{{\omega_1}^2 + {k_{out}}^2} \quad (1)$$

where f is the fraction of caged xenon and k_{out} the xenon out rate.

But directly quantifying the detectability of a host through the HyperCEST depolarization rate is a difficult task. Indeed in the case of cryptophanes and cucurbiturils the xenon in–out exchange rate depends on the guest/host concentration ratio, as a degenerate or kick-out exchange has been shown to occur.[30] The concentration of dissolved xenon being tricky to precisely determine, a large uncertainty may be introduced. Thus, we have preferred to use competition experiments with xenon host mixtures, and a dedicated pulse sequence using a fixed B_1 saturation simply placed at various frequency offsets (see Experimental). The limitation of this method is the prior knowledge of the Xe@host resonance frequencies (observable on ^{129}Xe spectra only at the highest concentrations), since at these low B_1 field amplitudes the saturation offset effect is important. Obviously a more sophisticated and accurate method such as the one proposed recently by Mitschang *et al.*[31] could have been used, but here the purpose is just a comparison between xenon hosts.

Fig. 4 displays the depolarization curves obtained for cryptophanes **1** and **2** with concentrations ranging from 5 μM to 50 nM in D_2O, using a saturation field strength of B_1 = 4.2 μT and a temperature of 298 K.

In order to perform the experiments in a more biological medium new cryptophane solutions have been prepared in PBS (phosphate buffer saline). Table 1 gives the corresponding xenon depolarization rates for various concentrations of hosts **1** and **2**. For each concentration, the depolarization rate is faster for Xe@**2** than for Xe@**1** by a factor between 3.5 and 5.9.

In a last step, we aimed to assess the detectability *via* ^{129}Xe NMR of cucurbit[6]uril **3**, using the same study protocol. Xenon in cucurbit[6]uril resonates at 127 ppm (see Fig. S16 of the ESI†), so it was not obvious to compare it with the *syn* cryptophane **2** because of the proximity of the resonance frequencies of xenon inside these two hosts (462 Hz). We instead turned to a **1**–**3** comparison. But we encountered several difficulties. First, while cryptophanes solubilize in water at slightly basic pH, cucurbiturils require the addition of cations such as Na_2SO_4.[32] Our first attempts to use a mother solution and successively dilute in D_2O gave unexpected results that precluded any quantitative interpretation. Fig. S17 of the ESI† shows the low field region of the ^{1}H NMR spectrum of a mixture of compound **1** (3.9 μM) and compound **3** (3.3 μM) and after dilution in D_2O by a factor 2. Clearly, while as expected a ratio of 2 is observed for the cryptophane, the ^{1}H signals of the curcurbituril vanish. This is probably due to the subsequent dilution of Na_2SO_4 and a too low ionic strength which favors the formation of cucurbit[6]uril aggregates.

Keeping constant the concentration of Na_2SO_4 in order to maintain a sufficiently high ionic strength for cucurbit[6]uril was questionable, as carboxylic acid (also present with carboxylate forms in the experimental conditions used) and sulfate groups are known to interact,[33] which could become problematic for the cryptophane. Thus, we turned to solutions in PBS, as previously for comparison between **1** and **2**. This solved the problem of the cucurbituril solubility and thereby enabled us to prepare solutions of equimolar concentrations of **1** and **3** at different dilutions (ESI,† Fig. S18).

While for comparison between the cryptophanes **1** and **2** the cage occupancy by xenon (the f term in eqn (1)) is almost the same, and thus λ_{on} directly derives from k_{out}, it is not the same situation for comparison between **1** and **3**. The xenon binding constant lower with cucurbit[6]uril than for cryptophanes makes that the occupancy factors can be quite different.

When the xenon host concentration diminishes, the f factor diminishes, while, due to the degenerate exchange, k_{out} increases. From eqn (1), Kunth and co-workers[34] distinguish two limit cases:

$$\text{Smatrong saturation } (\omega_1 \gg f{\cdot}k_{out}){:}\ \lambda_{on} \approx f{\cdot}k_{out} \quad (2)$$

$$\text{Weak saturation } (w_1 \ll f{\cdot}k_{out}){:}\ \lambda_{on} \approx \left(\frac{f}{k_{out}}\right){\omega_1}^2 \quad (3)$$

Thus, for strong saturation, the two effects act in opposite directions on the depolarization rate, *i.e.* a high depolarization rate could be induced by a high occupancy factor and a low xenon out rate. Also, increasing too much the saturation

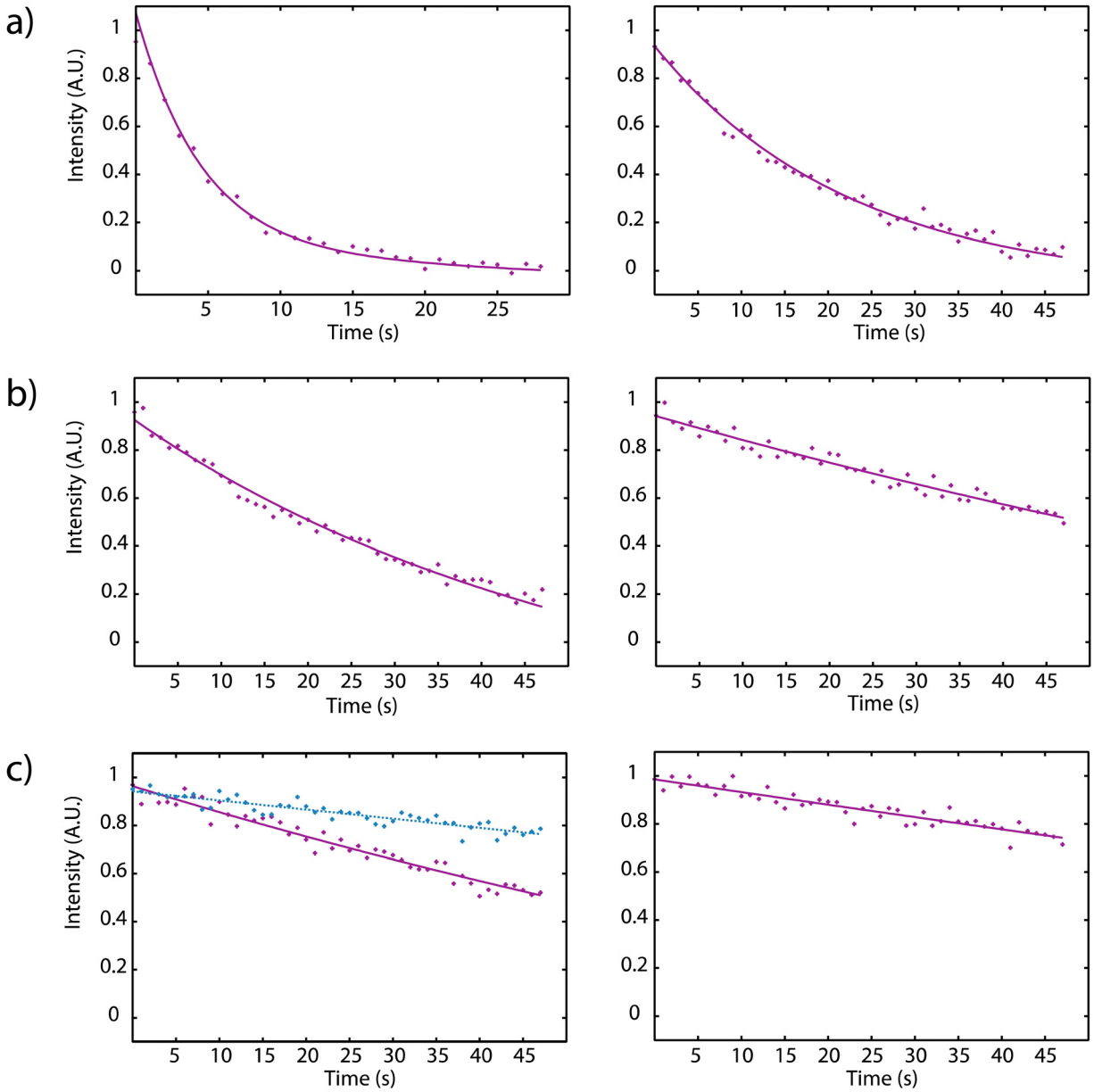

Fig. 4 Example of evolution curves of the ^{129}Xe magnetization after saturation at the frequency of Xe@**2** (left) and Xe@**1** (right) as a function of saturation time, for different cryptophane concentrations: (a) 5 μM, (b) 500 nM, (c) 50 nM, in D_2O. (a) Left: Note that due to a very fast magnetization loss with **2** at 5 μM, only the 28 first data points have been kept. In (c)-left, the data points obtained with off-resonance saturation (see text) and the corresponding best-fit curve are superimposed in blue.

Table 1 Depolarization rates for xenon in cryptophanes **1** and **2** in PBS. The saturation strength was 1.05 μT for the 5 and 2.5 μM solutions, and 2.1 μT for the other concentrations

Concentration (nM)	Depolarization rate Xe@**1** (s^{-1})	Depolarization rate Xe@**2** (s^{-1})
5000	0.3552 ± 0.0190	0.8236 ± 0.0658
2500	0.1146 ± 0.0021	0.4074 ± 0.0231
500	0.0373 ± 0.0030	0.2453 ± 0.0422
250	0.0435 ± 0.0042	0.2559 ± 0.0161
50	0.0268 ± 0.0004	0.1069 ± 0.0032

strength ω_1 can lead to crossover effect where the B_1 field directly affect the free xenon resonance frequency. In our method, we have thus chosen to keep ω_1 low (eqn (3)) so that the effects of variation of k_{out} and f are combined.

Table 2 gives the depolarization rates measured for xenon in anti-cryptophane **1** and cucurbit[6]uril **3** at different concentrations in PBS. Systematically, the depolarization rate is higher for Xe@**3** than for Xe@**1** by a factor between 1.8 and 2.6.

Experimental

Synthesis of compound *syn*-2

The compound *syn*-**2** was prepared in four steps from the known *syn*-cryptophane-**4** (C_3-symmetry) decorated with three

Table 2 Depolarization rates for xenon in hosts **1** and **3** in PBS. The saturation strength was 2.1 μT for the 4 and 0.8 μM solutions, and 4.2 μT for the other concentrations

Concentration (nM)	Depolarization rate Xe@**1** (s^{-1})	Depolarization rate Xe@**3** (s^{-1})
4000	0.3479 ± 0.0243	0.6175 ± 0.0349
800	0.0601 ± 0.0113	0.1366 ± 0.0248
400	0.0428 ± 0.0062	0.1112 ± 0.0136
200	0.0206 ± 0.0011	0.0508 ± 0.0029

hydroxyl functions on one CTB cap and three protected hydroxyl groups on the other CTB cap (see Fig. S1 of the ESI†). Three ester functions were first introduced by reacting compound *syn*-**4** with an excess of methyl bromoacetate at 60 °C in the presence of a base in DMF to give rise to compound *syn*-**5** in 68% yield. Removal of the three benzyl groups was then achieved by reacting *syn*-**5** in the presence of a palladium catalyst with hydrogen gas in a CH_2Cl_2/CH_3OH mixture. The procedure provided compound *syn*-**6** in quantitative yield. Three additional ester groups were then grafted on the cryptophane skeleton with 82% yield by reacting *syn*-**6** in the presence of an excess of methyl bromoacetate as reported for the preparation of compound *syn*-**5**. Finally, the resulting *syn*-**7** derivative was subjected to hydrolysis under basic conditions followed by acidification with concentrated HCl to give the expected *syn*-**2** compound in 79% yield (isolated). It was noticed that compound *syn*-**2** shows lower solubility in DMSO and water than its congener *anti*-**1** under similar conditions. Compound *syn*-**2** (C_{3h} symmetry) was fully characterized by ^{1}H, ^{13}C NMR spectroscopy (see Fig. S2–S4 of the ESI†) and HRMS. ^{1}H NMR (500 MHz, D_2O, 298 K): d 7.04 (s, 6H), 6.83 (s, 6H), 4.61 (d, 6H, J = 14 Hz), 4.57 (d, 6H, J = 15 Hz), 4.50 (q, 6H, J = 10 Hz, J = 4 Hz), 4.19 (d, 6H, J = 15 Hz), 4.01 (q, 6H, J = 10 Hz, J = 4 Hz), 3.43 (d, 6H, J = 14 Hz). ^{13}C{^{1}H} NMR (125.7 MHz, D_2O, 298 K): d 178.0 (6C), 148.2 (6C), 146.0 (6C), 136.3 (6C), 134.7 (6C), 119.7 (6C), 116.0 (6C), 69.5 (6C), 69.2 (6C), 36.5 (6C). HRMS (ESI) m/z: $[M + Na]^+$ calcd for $C_{60}H_{54}NaO_{24}$: 1181.2897; found: 1181.2892.

Preparation of the xenon host solutions for NMR

For the ^{1}H–^{13}C HSQC and HMBC experiments, 4.48 mg of *syn*-cryptophane **2** were dissolved in 600 μL D_2O and 20 μL NaOD 0.1 M. In a second step, for the competition experiments in water, stock solutions were prepared. For the first one, 0.71 mg of *anti*-cryptophane **1** was dissolved in 600 μL D_2O with 3 μL NaOD 0.1 M. For the second one, 0.69 mg of *syn*-cryptophane **2** was dissolved in 600 μL D_2O with 3 μL NaOD 0.1 M. 300 μL of each solution was then added in a tube to provide the mother solution of the cryptophane mixture. Then successive dilutions gave the concentrations wished for the ^{129}Xe depolarization experiments. Thirdly, for the study of the xenon hosts in a more biological medium, they have been dissolved in a PBS buffer made of 20 mM sodium phosphate + 150 mM NaCl in D_2O for a pH of 7.4. 0.81 mg of *anti*-cryptophane **1** was dissolved in 600 μL of the same buffer, and 0.84 mg of *syn*-cryptophane **2** was dissolved in 600 μL of PBS. Then successive dilutions gave the concentrations wished for the ^{129}Xe depolarization experiments.

For the competition experiments with cucurbit[6]uril **3**, a mother solution was prepared by dissolving 0.42 mg of this molecule in 600 μL of PBS buffer.

Introduction of hyperpolarized xenon

All the ^{129}Xe NMR spectra and all the ^{129}Xe exchange experiments were performed with hyperpolarized xenon. Laser-polarized xenon was produced in the batch mode, using our home-built apparatus described in ref. 35. Due to issues related to the laser source the current average polarization was only *ca.* 5%. Then it was transported in the frozen state to the NMR spectrometer and transferred *via* a vacuum line in the fringe field of the magnet to the NMR tube equipped with a screw-cap and a J. Young valve. In this purpose the NMR tube was previously degassed and a cold point was created by the use of a dedicated hollow spinner. In this way, xenon condensed on top of the solution, without significantly cooling it. The NMR tube was then vigorously shaken in order to speed up the xenon dissolution. A delay of 10 seconds before the acquisition was systematically set. The amount of xenon inside the NMR tube was estimated by weighting the tube after degassing and after xenon introduction.

^{1}H, ^{13}C and ^{129}Xe NMR experiments

Except otherwise indicated, all NMR experiments were performed at 11.7 T and 298 K with a Bruker 5 mm-broadband inverse probehead equipped with z gradient. The radiofrequency field strength on the ^{129}Xe channel was calibrated using a reference tube containing molar concentration of xenon in dodecane.

Measurement of the ^{129}Xe depolarization rates

In this purpose a specific NMR pulse sequence, depicted in ESI† (Fig. S19), was conceived. This pseudo-2D sequence starts by a read pulse of small flip angle θ. Then after detection, which provides the first data point at time 0, saturation occurs at a chosen frequency. Saturation is achieved by one hundred repetitions (n = 100) of D-Snob pulses of 10 ms duration. Then, detection is achieved after a small flip angle read pulse. The pulse program loops 48 times (td1 = 48) on the 'read pulse – detection – saturation' sequence. For the sake of speed, there is no interscan delay and the data are only written on the disk at the end of the sequence. In order to enable a short acquisition time and thus a short interscan delay (34 ms), a magnetic field gradient of 2 mT m^{-1} is applied during detection, and a purge gradient of random amplitude is applied between each loop. According to the xenon host concentration, the saturation rf strength is adjusted between ν_1 = 12.5 Hz (B_{1sat} = 1.05 μT) and ν_1 = 50 Hz (B_{1sat} = 4.2 μT).

Rigorously, three effects should be considered to account for the magnetization loss during the sequence: relaxation, rf pulse and exchange. Dealing with relaxation, considering that xenon relaxes in a similar rate in **1** and in **2**, a term in $\exp(-t/T_{1eff})$

occurs, with $\frac{1}{T_{1\text{eff}}} = f'\frac{1}{T_{1\text{bound}}} + (1-f')\frac{1}{T_{1\text{free}}}$, where f' is the fraction of bound xenon: $f' = \frac{[\text{Xe@}\mathbf{1}] + [\text{Xe@}\mathbf{2}]}{[\text{Xe}]_{\text{total}}}$.

For the effect of the rf pulse, the theoretical curve for a pulse of 4° flip angle is a straight line of slope $s = -0.00257$ (*cf.* Fig. S20 of the ESI†). The exchange term finally is expressed as an exponential decay $\exp(-k_{\text{ex}}t)$, where k_{ex} is the exchange rate. But one can consider that at current cryptophane concentrations used for the exchange experiments (10^{-5} to 10^{-8} M), and given the concentration of dissolved xenon (in the millimolar range), one can neglect the relaxation. Thus for the depolarization experiments the data points obey a recursive law in $S(x) = (S(x-1) + s)\cdot\exp(-k_{\text{ex}}\Delta t)$ with $S(0) = 1$. A value of 10958 Hz separates the frequency of xenon caged in **2** from that of free xenon ($\Delta\nu_2 = \delta_{\text{free}} - \delta_{\text{Xe@2}} = -10\,958$ Hz) and 17 989 Hz separate the frequency of xenon caged in **1** from it ($\Delta\nu_1 = -17\,989$ Hz). For each of the cryptophane concentration, in order to check that no cross-over effect can perturb the result, an 'off-resonance' experiment was performed in which saturation is applied at an offset symmetrical to $\Delta\nu_2$ with respect to the frequency of free xenon ($\Delta\nu_{\text{off}} = +10\,958$ Hz). The same protocol (fit *etc.*) was used for comparison between cucurbit[6]uril **3** and *anti*-cryptophane **1**. 9480 Hz separate the frequency of xenon complexed with 3 from that of free xenon ($\Delta\nu_3 = -9480$ Hz). The depolarization rates given in Tables 1 and 2 are the means of three measures, with standard deviations.

Conclusions

Until now the synthesis of *syn*-cryptophanes with small cavities was challenging. But the advent of new methods, such as the use of 1,1,1,3,3,3-hexafluoroisopropanol as co-solvent and the recent synthesis of functionalized *syn*-cryptophanes with C_3-symmetry,[23,36] has facilitated their production and opens new doors, in particular for the conception of ^{129}Xe NMR-based biosensors. Interestingly, the second approach seems well suited for the design of these biosensors since the starting material used for the synthesis of *syn*-cryptophane **2** has lower symmetry and reactive phenolic functions that can be directly engaged to graft water-soluble groups and ligands aimed at recognizing a biological target.

This represents a major asset. Indeed, ^{129}Xe NMR-based biosensors made from *anti*-cryptophanes usually require additional chemical transformations to introduce water-solubilizing substituents. Here, compounds **4** and **6** (see Fig. S1, ESI†) appear as ideal host molecules to prepare rapidly biosensors. Progress is underway to further improve the synthesis of these *syn* intermediates.

The newly synthesized *syn*-cryptophane **2** is the first member of a family of water-soluble xenon hosts with very singular characteristics. Its properties, as well as those of its complex with xenon, make it a very attractive candidate for ^{129}Xe NMR-based biosensing. Firstly, as the resonance frequency of xenon in **2** differs drastically from that of xenon in **1** – more than 50 ppm (or 7000 Hz at 11.7 Tesla) – this can allow interesting multiplexing experiments,[37] even at low magnetic field.[38] Secondly, from a structural point of view, when dissolved in water it is exempt of forms not able to encapsulate xenon. In that it is superior to *anti*-**1** and to several *anti*-cryptophanes in general. Thirdly, it does not complex dissolved oxygen, which represents an advantage over cryptophane *anti*-**1**. Fourthly, it shows a high binding constant with xenon, which means that there are less competitors for encapsulation in solution. For instance, although this has not been extensively tested, at the difference of cucurbit[6]uril **3**, it does not complex anions. Note that while cryptophane **2** is slightly soluble in water at neutral pH, cucurbit[6]uril needs the addition of salts to become soluble. Last but not least, the xenon in–out exchange with *syn*-cryptophane **2** is faster than with *anti*-**1**, by a factor *ca.* 6 at low cryptophane concentration. Even if it was not a question here of trying to reach the lowest detection threshold (at lower cryptophane concentration we could use a stronger rf saturation without crossover effect), we have shown that its molar detectivity is much higher. All together the *syn*-**2** compound and the *syn*-congeners in general appear to be an excellent basis for designing new ^{129}Xe NMR-based biosensors with superior characteristics to its *anti*-congener, in particular an efficient xenon turnover. Obviously other systems such as gas vesicles are performing well for sensitive xenon detection,[39] but with a view to building bioprobes composed of a xenon host and a recognition antenna, *syn* cryptophanes are very promising. In the context of the search for an ultimate detection they could constitute the elementary brick of dendrimers for example.[40]

Author contributions

T. B. synthesized the cryptophanes **1** and **2**. P. B. conceived the ^{129}Xe NMR approach to evaluate the exchange rate and wrote the pulse sequence. E. L. prepared the xenon host solutions. E. L. and P. B. performed the ^{129}Xe NMR experiments and processed the data. P. B. wrote the initial version of the manuscript. All authors have given their approval to the final version of the manuscript.

Conflicts of interest

There are no conflicts to declare.

Acknowledgements

The French National Research Agency (ANR) is acknowledged for financial support (Project ANR19-CE19 0024 PHOENIX).

Notes and references

1 M. M. Spence, S. M. Rubin, I. E. Dimitrov, E. J. Ruiz, D. E. Wemmer, A. Pines, S. Q. Yao, F. Tian and P. G. Schultz, *Proc. Natl. Acad. Sci. U. S. A.*, 2001, **98**, 10654–10657.

2 P. Berthault, G. Huber and H. Desvaux, *Prog. Nucl. Magn. Reson. Spectrosc.*, 2009, **55**, 35–60.
3 J. Jayapaul and L. Schröder, *Molecules*, 2020, **25**, 4627–4722.
4 C. Boutin, A. Stopin, F. Lenda, T. Brotin, J.-P. Dutasta, N. Jamin, A. Sanson, Y. Boulard, F. Leteurtre, G. Huber, A. Bogaert-Buchmann, N. Tassali, H. Desvaux, M. Carrière and P. Berthault, *Bioorg. Med. Chem.*, 2011, **19**, 4135–4143.
5 G. K. Seward, Y. Bai, N. S. Khan and I. J. Dmochowski, *Chem. Sci.*, 2011, **2**, 1103–1110.
6 C. Witte, V. Martos, H. M. Rose, S. Reinke, S. Klippel, L. Schröder and C. P. R. Hackenberger, *Angew. Chem., Int. Ed.*, 2015, **54**, 2806–2810.
7 G. Milanole, B. Gao, A. Paoletti, G. Pieters, C. Dugave, E. Deutsch, S. Rivera, F. Law, J.-L. Perfettini, E. Mari, E. Léonce, C. Boutin, P. Berthault, H. Volland, F. Fenaille, T. Brotin and B. Rousseau, *Bioorg. Med. Chem.*, 2017, **25**, 6653–6660.
8 N. Tassali, N. Kotera, C. Boutin, E. Léonce, Y. Boulard, B. Rousseau, E. Dubost, F. Taran, T. Brotin, J.-P. Dutasta and P. Berthault, *Anal. Chem.*, 2014, **86**, 1783–1788.
9 K. Jeong, C. C. Slack, C. C. Vassiliou, P. Dao, M. D. Gomes, D. J. Kennedy, A. E. Truxal, L. J. Sperling, M. B. Francis, D. E. Wemmer and A. Pines, *Chem. Phys. Chem.*, 2015, **16**, 3573–3577.
10 Q. Guo, Q. Zeng, W. Jiang, X. Zhang, Q. Luo, X. Zhang, L.-S. Bouchard, M. Liu and X. Zhou, *Chem. – Eur. J.*, 2016, **22**, 3967–3970.
11 S. Yang, W. Jiang, L. Ren, Y. Yuan, B. Zhang, Q. Luo, Q. Guo, L.-S. Bouchard, M. Liu and X. Zhou, *Anal. Chem.*, 2016, **88**, 5835–5840.
12 F. Schilling, L. Schröder, K. K. Palaniappan, S. Zapf, D. E. Wemmer and A. Pines, *Chem. Phys. Chem.*, 2010, **11**, 3529–3533.
13 E. Léonce, J.-P. Dognon, D. Pitrat, J.-C. Mulatier, T. Brotin and P. Berthault, *Chem. – Eur. J.*, 2018, **24**, 6534–6537.
14 P. Berthault, H. Desvaux, T. Wendlinger, M. Gyejacquot, A. Stopin, T. Brotin, J.-P. Dutasta and Y. Boulard, *Chem. – Eur. J.*, 2010, **16**, 12941–12946.
15 G. Huber, T. Brotin, L. Dubois, H. Desvaux, J.-P. Dutasta and P. Berthault, *J. Am. Chem. Soc.*, 2006, **128**, 6239–6246.
16 L. Schroder, T. J. Lowery, C. Hilty, D. E. Wemmer and A. Pines, *Science*, 2006, **314**, 446–449.
17 M. El Haouaj, M. Luhmer, Y. H. Ko, K. Kim and K. Bartik, *J. Chem. Soc., Perkin Trans. 2*, 2001, 804–807.
18 B. S. Kim, Y. H. Ko, Y. Kim, H. J. Lee, N. Selvapalam, H. C. Lee and K. Kim, *Chem. Commun.*, 2008, 2756–2758.
19 J. A. Finbloom, C. C. Slack, C. J. Bruns, K. Jeong, D. E. Wemmer, A. Pines and M. B. Francis, *Chem. Commun.*, 2016, **52**, 3119–3122.
20 Y. Wang and I. J. Dmochowski, *Chem. Commun.*, 2015, **51**, 8982–8985.
21 F. T. Hane, T. Li, P. Smylie, R. M. Pellizzari, J. A. Plata, B. DeBoef and M. S. Albert, *Sci. Rep.*, 2017, **7**, 41027.
22 C. T. McHugh, M. Kelley, N. J. Bryden and R. T. Branca, *Magn. Reson. Med.*, 2022, **87**, 1480–1489.
23 T. Brotin, E. Jeanneau, P. Berthault, E. Léonce, D. Pitrat and J.-C. Mulatier, *J. Org. Chem.*, 2018, **83**, 14465–14471.
24 M. Doll, P. Berthault, E. Léonce, C. Boutin, T. Buffeteau, N. Daugey, N. Vanthuyne, M. Jean, T. Brotin and N. De Rycke, *J. Org. Chem.*, 2021, **86**, 7648–7658.
25 M. Doll, P. Berthault, E. Léonce, C. Boutin, E. Jeanneau, T. Brotin and N. De Rycke, *J. Org. Chem.*, 2022, **87**, 2912–2920.
26 G. Huber, F.-X. Legrand, V. Lewin, D. Baumann, M.-P. Heck and P. Berthault, *Chem. Phys. Chem.*, 2011, **12**, 1053–1055.
27 L. Schroder, T. J. Lowery, C. Hilty, D. E. Wemmer and A. Pines, *Science*, 2006, **314**, 446–449.
28 M. Zaiss, M. Schnurr and P. Bachert, *J. Chem. Phys.*, 2012, **136**, 144106.
29 M. Kunth, C. Witte and L. Schröder, *J. Chem. Phys.*, 2014, **141**, 194202.
30 S. Korchak, W. Kilian, L. Schröder and L. Mitschang, *J. Magn. Reson.*, 2016, **265**, 139–145.
31 L. Mitschang, S. Korchak, W. Kilian and T. Riemer, *Anal. Chem.*, 2022, **94**, 2561–2568.
32 Y.-M. Jeon, J. Kim, D. Whang and K. Kim, *J. Am. Chem. Soc.*, 1996, **118**, 9790–9791.
33 A. Hopkins and A. Williams, *J. Org. Chem.*, 1982, **47**, 1745–1750.
34 M. Kunth, C. Witte and L. Schröder, *NMR Biomed.*, 2015, **28**, 601–606.
35 C. Chauvin, L. Liagre, C. Boutin, E. Mari, E. Léonce, G. Carret, B. Coltrinari and P. Berthault, *Rev. Sci. Instrum.*, 2016, **87**, 016105.
36 O. Della-Negra, Y. Cirillo, T. Brotin, J.-P. Dutasta, P.-L. Saaidi, B. Chatelet and A. Martinez, *Chem. Commun.*, 2022, **58**, 3330–3333.
37 P. Berthault, A. Bogaert-Buchmann, H. Desvaux, G. Huber and Y. Boulard, *J. Am. Chem. Soc.*, 2008, **130**, 16456–16457.
38 K. Chighine, E. Léonce, C. Boutin, H. Desvaux and P. Berthault, *Magn. Reson.*, 2021, **2**, 409–420.
39 M. G. Shapiro, R. M. Ramirez, L. J. Sperling, G. Sun, J. Sun, A. Pines, D. V. Schaffer and V. S. Bajaj, *Nat. Chem.*, 2014, **6**, 629–634.
40 J. L. Mynar, T. J. Lowery, D. E. Wemmer, A. Pines and J. M. J. Fréchet, *J. Am. Chem. Soc.*, 2006, **128**, 6334–6335.